Spectroscopic Imaging of Single Atoms Within a Bulk Solid

M. Varela,[1] S. D. Findlay,[2] A. R. Lupini,[1] H. M. Christen,[1] A. Y. Borisevich,[1] N. Dellby,[3] O. L. Krivanek,[3] P. D. Nellist,[3]
M. P. Oxley,[2] L. J. Allen,[2] and S. J. Pennycook[1]

[1]*Condensed Matter Sciences Division, Oak Ridge National Laboratory, P.O. Box 2008, Oak Ridge, Tennessee 37831-6030, USA*
[2]*School of Physics, University of Melbourne, Victoria 3010, Australia*
[3]*Nion Co., 1102 8th Street, Kirkland, Washington 98033, USA*
(Received 5 December 2003; published 3 March 2004)

The ability to localize, identify, and measure the electronic environment of individual atoms will provide fundamental insights into many issues in materials science, physics, and nanotechnology. We demonstrate, using an aberration-corrected scanning transmission electron microscope, the spectroscopic imaging of single La atoms inside $CaTiO_3$. Dynamical simulations confirm that the spectroscopic information is spatially confined around the scattering atom. Furthermore, we show how the depth of the atom within the crystal may be estimated.

Detection and measurement of the response of individual atoms has become a challenging issue to provide new insight into many fields in condensed matter and nanoscale sciences. Distributions of isolated atoms deeply modify the physical properties of many of the technologically most relevant and scientifically most interesting materials. Therefore, analytical techniques capable of probing single-atom identity and location are increasingly in demand. Here we show how the aberration-corrected scanning transmission electron microscope (STEM) allows not only the imaging of individual atoms inside a crystal, but their spectroscopic identification, with spatial resolution at the atomic scale. This substantial improvement in sensitivity opens up the possibility of probing the electronic environment of a single atom. Furthermore, by comparing signals from columns adjacent to that containing the single atom with dynamical simulations, the depth of the atom in the crystal can be estimated.

Much of the reported work on the identification and imaging of single atoms has been achieved by indirect techniques such as image simulation, including complex reconstruction of phase images with through focal series restoration [1,2]. The STEM provides direct images of individual atoms as first demonstrated many years ago by the imaging of individual U and Th atoms on a thin carbon film [3]. More recently, at a resolution of ~0.13 nm, the STEM has successfully imaged single atoms on and within a variety of materials, including catalysts [4] and semiconductors [3,5,6]. Although the optics of the STEM is ideally suited to simultaneous imaging and spectroscopy, very few results have been reported that combine direct imaging with spectroscopic identification of individual atoms. Electron energy loss spectroscopy (EELS) signals also display high spatial resolution. Subunit cell analysis was first achieved by Spence and Lynch [7] at 1.1 nm resolution. Single Gd atoms were, for the first time, identified by Suenaga and co-workers [8] by combining phase contrast TEM imaging with EELS mapping in the STEM. However, their EELS resolution was only 0.6 nm, sufficient to resolve their widely spaced Gd atoms but insufficient to resolve the atomic structure of most materials. Scanning probe microscopies have also succeeded in achieving atomic-resolution spectroscopic identification of single atoms on surfaces, but they cannot probe individual atoms within the bulk environment.

Recent advances in aberration-corrected STEM provide the perfect scenario to address such a problem [9]. A Z-contrast image is obtained by collecting, point by point, the Rutherford-scattered electrons at high angles using a high angle annular dark field (HAADF) detector. Energy loss electrons passing through the central hole in the detector can be collected simultaneously with the HAADF image. This correlation allows EELS to be performed with atomic resolution [10–12], limited only by the size of the probe [13,14]. Recently, by correcting the aberrations of the STEM probe-forming lens, a subangstrom beam has been demonstrated on a VG Microscopes HB501UX field emission STEM operating at 120 kV which is equipped with a Nion aberration corrector [15]. In a similar microscope, operated at 100 kV, a spatial resolution close to 0.11 nm is routinely achieved, and in this Letter we show how this enables us not only to image an individual atom within a crystal but to identify it spectroscopically.

The superlattice sample used for this study was a stack of $CaTiO_3$ and $La_xCa_{1-x}TiO_3$ layers with a very low concentration of La dopants, prepared by pulsed laser deposition at 800 °C, in an O_2 pressure of 75 mTorr, with a laser energy of 3 J/cm^2 at 248 nm and a repetition rate of 10 Hz. One commercial $CaTiO_3$ target and a specially prepared $La_xCa_{1-x}TiO_3$ target with $x = 0.04 \pm 0.002$ were used. The sample is epitaxial and highly ordered, and contains reference layers of $La_{0.04}Ca_{0.96}TiO_3$ approximately 2.3 nm thick grown using 100 shots of the La-doped target. Layers with correspondingly lower La concentrations were grown by using fewer

shots, and were correspondingly thinner. From this calibration we calculate that a layer grown using just a single shot results in a La concentration of one atom per 60 nm^2. Assuming a typical TEM cross-section specimen to be about 10 nm thick, on average, one La atom should be found every 16 ± 4 unit-cell columns. Simple statistical arguments yield a probability of only 3% that any given La-containing column contains more than one La atom. Such cross-section specimens were prepared by conventional methods. To minimize surface damage the final cleaning was performed by ion milling at 0.5 kV. Plasma cleaning was also used to prevent sample contamination.

Figure 1 shows a high resolution Z-contrast image of a $La_{0.002}Ca_{0.998}TiO_3$ layer adjacent to a thicker $La_{0.04}Ca_{0.96}TiO_3$ layer. The higher atomic number of La, as opposed to Ca, O, or Ti, makes single La atoms appear as bright spots in this environment, although this brightness is dependent on atom depth [16,17]. Figure 1(b) shows the intensity traces across the atom. While we cannot completely exclude the possibility that any particular column contains two La atoms, many other single La atoms were imaged at different positions of the sample, in order to get better statistics, most giving an increase in columnar intensity by $\sim 10\%$. They are seen to sit on the Ca site of the $La_xCa_{1-x}TiO_3$ perovskite structure, easily identifiable due to the fact that Ca columns appear darker than TiO columns.

Identification of the atoms was carried out using a McMullan design charge-coupled device parallel-detection EELS system [18]. This system does not provide optimized coupling from the aberration-corrected beam, having a collection efficiency of only 8%. [Collection efficiency is calculated as $\beta^2/(\alpha^2 + \theta_E^2)$, where $\beta =$

7 mrad is the spectrometer entrance aperture, $\alpha = 25$ mrad is the probe-forming aperture, and $\theta_E = \Delta E/2E_0$ is the characteristic angle of inelastic scattering for an energy loss ΔE and incident energy E_0.] Nevertheless, by scanning the STEM probe directly over a highly magnified image of an isolated La atom (0.1 nm $\times$ 0.1 nm in size as shown in Fig. 2), a clear EELS signature is obtained. In Fig. 2, spectrum 3 shows two distinct peaks that correspond to the La $M_{4,5}$ lines at 832 and 849 eV. The intensity is low, as one would expect from the small number of counts associated with the excitations of a single atom, but clearly observable. The total number of $M_{4,5}$ excitations for this spectrum is of the order of 10^4. To be certain that a single La atom can be detected, ten different bright spots were analyzed and each showed characteristic La lines with similar intensity. No meaningful beam damage was observed during the acquisition times employed, which were of the order of tenths of seconds.

There has been much discussion about detection limits and the role that the delocalization of the underlying ionization process plays in limiting the resolution of the STEM image [7,13,14,19–21]. To analyze the localization of the EELS signal we have taken spectra with the probe positioned on nearby columns as indicated in Fig. 2(a). Given the fact that neighboring atomic columns (2 and 4) correspond to different atomic species (TiO and O columns), the channeling and therefore the localization of the signal would be different. As depicted in Fig. 2(b), the EELS signal attributed to the La single atom is clearly
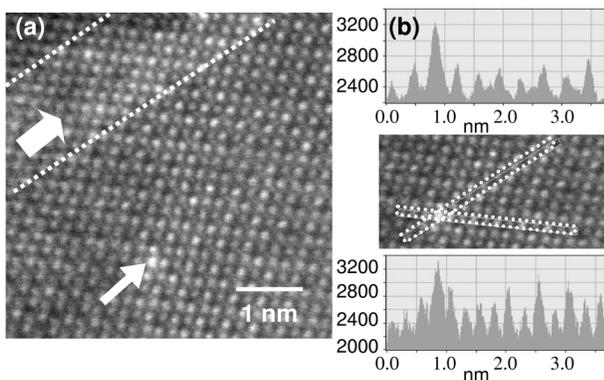

FIG. 1. (a) Z-contrast image showing an individual La atom, marked by a thin arrow. The reference $La_{0.04}Ca_{0.96}TiO_3$ layer is marked with a thick arrow and the interfaces are marked with dotted lines. (b) Intensity profiles in the [100] and [110] directions (top and bottom, respectively). Column-to-column fluctuations are visible due to ion milling surface damage, but the La atom is clearly identifiable and seen to be located on a Ca site. Image obtained with probe current of approximately 100 pA over 10 s.
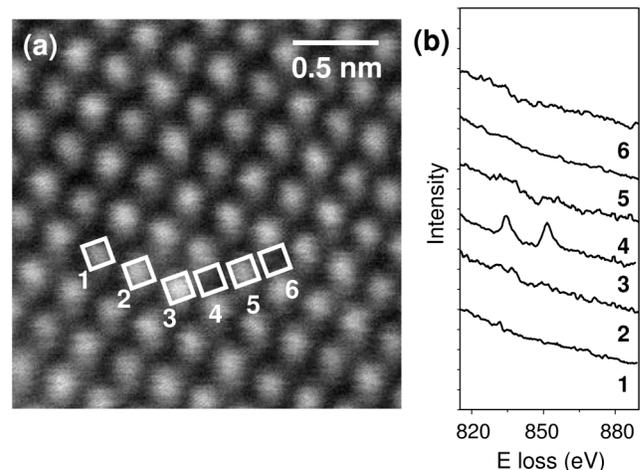
FIG. 2. (a) Z-contrast image with (b) EELS traces showing spectroscopic identification of a single La atom at atomic spatial resolution, with the same beam used for imaging. The $M_{4,5}$ lines of La are seen strongly in spectrum 3 obtained from the bright column at 2×10^7 magnification and a total collection time of 30 s. Other spectra from neighboring columns show much reduced or undetectable La signal. These spectra were obtained with collection times of 20 s, and are shown normalized to the preedge intensity and displaced vertically for clarity.

localized on the atomic column containing this ion. When the electron beam is placed on adjacent columns the signal is substantially reduced, to only $10 \pm 5\%$ on the neighboring TiO column (labeled 2), and to $20 \pm 5\%$ on the neighboring O site (labeled 4), only 0.19 nm away. This clearly indicates that the La can be localized within significantly better than 0.2 nm, which is much larger than the impact parameter for La-M excitation [13] and therefore suggests that the residual intensity from neighboring columns is almost certainly the effect of channeling [22].

To explore the role of channeling, dynamical diffraction calculations were performed. Figure 3(a) shows the simulated La signal strength for an aberration-free probe situated on the Ca column, O column, and TiO column as a function of the impurity depth. A simplified cubic model for the structure suffices for this estimate, but subsequent calculations are based upon the distorted perovskite structure [23]. The contribution on the Ca column initially increases due to the electrostatic attraction to the column (channeling), but then decreases as elastic and inelastic scattering mechanisms broaden the probe. The contribution on the O column rises gradually; simulations of the electron density make clear that this is due to probe spreading. From this figure it is estimated that a $20 \pm 5\%$ signal on the O column is obtained with an impurity depth of around 10 nm. The lack of any appreciable signal from the TiO column is an expression of the channeling strength of this column. To explain the $10 \pm 5\%$ signal measured it must be appreciated that in the experiment the probe was not situated upon a single point but raster scanned across a highly magnified image. This introduces a finite, square scan region, of approximately 0.1 nm side length. Figures 3(b) and 3(c) show the HAADF images simulated [22,24] for a 15 nm thick crystal using an aberration-free probe and an aberration-balanced probe, respectively. The latter uses parameters measured from autotuning which, though recorded on a different occasion, can be regarded as typical. The latter image has been convolved with a Gaussian of half-width 0.04 nm, accounting for position instability of the probe and finite source size [25]. EELS images were simulated using mixed dynamic form factor theory [24,26].

Figures 3(d) and 3(e) show EELS images corresponding to the parameters used in Figs. 3(b) and 3(c). The asymmetry of the structure, particularly whereby O columns distorted towards the Ca column provide a stronger signal than those distorted away from it, is evident. Figure 3(f) shows the scan regions and the signal strengths therein as a percentage of that on the Ca column. In these simulations the impurity was set at a depth of 12.2 nm. Note that the O column signal strength is on average higher than that of the experiment, and the TiO column signal strength is on average lower. For the second probe there are columns which agree with the experimental results to within the error bars. While the
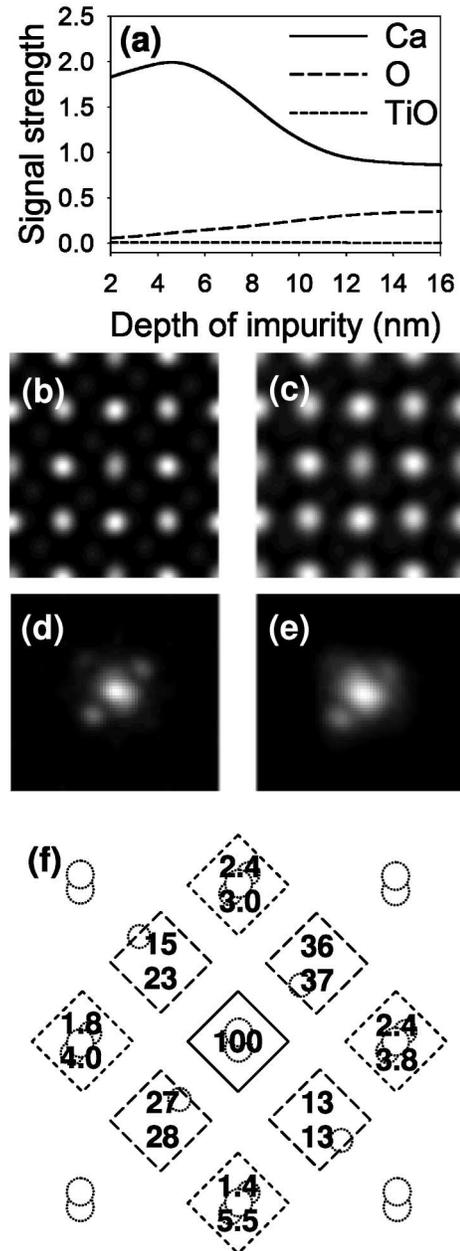

FIG. 3. Simulated HAADF and EELS images. (a) Depth dependence of La signal strength on the different columns using simple cubic perovskite structure. (b) HAADF image with aberration-free probe. (c) HAADF image with aberration-balanced probe and 0.04 nm Gaussian broadening. (d) EELS image corresponding to probe of (b). (e) EELS image corresponding to probe of (c). (f) Signal strength in raster scan regions as a percentage of that on central Ca column. The top number refers to aberration-free probe. The bottom number refers to aberration-balanced probe. The boundaries of the scan regions refer to the legend in (a).

parameters used may not correspond precisely to those characterizing the experiment, the simulations have elucidated the mechanism by which the signals are obtained. The simulations support the localization of the ionization

interaction and demonstrate that the dynamical propagation, in transferring some electron intensity to adjacent columns, is responsible for the signals obtained. The depth dependence seen in Fig. 3(a) is suggestive. It will be interesting to investigate how accurately the depth of an impurity atom may be determined in this fashion, particularly using larger probe-forming apertures and variable defocus.

In summary, an individual atom within a bulk solid has been identified spectroscopically with spatial resolution at the atomic level. This not only allows the detection and identification of single atoms, but also measurement of their electronic properties. Through dynamical simulations of probe spreading, an indication of atom depth is also obtained. Furthermore, the local formal oxidation state can be determined from the ratio of white line features present in L edges giving direct information about the magnetic moment and the valence of the atom. The present statistics are sufficient for such an analysis, although in this case the La ion is known to have a fixed 3+ valence state. However, optimum coupling of the aberration-corrected beam into the spectrometer would not only improve collection efficiency by over an order of magnitude, but also allow correction of spectrometer aberrations to give improved energy resolution [27]. This would allow better comparison of local electronic structure with first-principles calculations [28].

There are many situations where the valence state of localized impurity atoms is variable, and it is very often the critical factor controlling macroscopic properties. Examples include band-bending effects at grain boundaries [29,30], charge ordering in perovskite-based oxides [31], charge-modulation superlattices [32], and molecular species in nanotubes [33,34]. We anticipate single-atom analysis will open up many other areas of science where isolated atoms control macroscopic phenomena, including the origin of ductility or embrittlement in structural alloys, the nature of trap states at semiconductor interfaces, luminescent quantum efficiency in nanocrystals, and active sites in heterogeneous catalysts.

The single atom represents the smallest quantum of matter that retains the characteristics of the material through its local electronic environment. The ability to probe the electronic structure of a material at this level represents the ultimate advance for understanding the atomic origins of materials properties. This work opens up this possibility.

[1]   C. L. Jia, M. Lentzen, and K. Urban, Science **299**, 870 (2003).
[2]   R. R. Meyer *et al.*, Science **289**, 1324 (2000).
[3]   A. V. Crewe, J. Wall, and J. Langmore, Science **168**, 1338 (1970).
[4]   P. D. Nellist and S. J. Pennycook, Science **274**, 413 (1996).
[5]   P. M. Voyles *et al.*, Nature (London) **416**, 826 (2002).
[6]   A. R. Lupini and S. J. Pennycook, Ultramicroscopy **96**, 313 (2003).
[7]   J. C. H. Spence and J. Lynch, Ultramicroscopy **9**, 267 (1982).
[8]   K. Suenaga *et al.*, Science **290**, 2280 (2000).
[9]   N. Dellby *et al.*, J. Electron Microsc. **50**, 177 (2001).
[10] N. D. Browning, M. F. Chisholm, and S. J. Pennycook, Nature (London) **366**, 143 (1993).
[11] G. Duscher, N. D. Browning, and S. J. Pennycook, Phys. Status Solidi A **166**, 327 (1998).
[12] U. Kaiser *et al.*, Nature Materials **1**, 102 (2002).
[13] B. Rafferty and S. J. Pennycook, Ultramicroscopy **78**, 141 (1999).
[14] L. J. Allen *et al.*, Phys. Rev. Lett. **91**, 105503 (2003).
[15] P. E. Batson, N. Dellby, and O. L. Krivanek, Nature (London) **418**, 617 (2002).
[16] P. D. Nellist and S. J. Pennycook, Adv. Imag. Electr. Phys. **113**, 147 (2000).
[17] K. Nakamura *et al.*, J. Electron Microsc. **46**, 33 (1997).
[18] D. McMullan *et al.*, Inst. Phys. Conf. Ser. **98**, 55 (1990).
[19] H. Kohl and H. Rose, Adv. Imag. Electr. Phys. **65**, 173 (1985).
[20] D. A. Muller and J. Silcox, Ultramicroscopy **59**, 195 (1995).
[21] O. F. Holbrook and D. M. Bird, Inst. Phys. Conf. Ser. **147**, 145 (1995).
[22] L. J. Allen *et al.*, Ultramicroscopy **96**, 47 (2003).
[23] R. H. Buttner and E. N. Maslen, Acta Crystallogr. Sect. B **48**, 644 (1992).
[24] S. D. Findlay *et al.*, Ultramicroscopy **96**, 65 (2003).
[25] P. D. Nellist and J. M. Rodenburg, Ultramicroscopy **54**, 61 (1994).
[26] M. P. Oxley and L. J. Allen, Phys. Rev. B **57**, 3273 (1998).
[27] N. Dellby *et al.*, Microscopy and Microanalysis (to be published).
[28] R. Buczko *et al.*, Phys. Rev. Lett. **85**, 2168 (2000).
[29] M. Kim *et al.*, Phys. Rev. Lett. **86**, 4056 (2001).
[30] H. Hilgenkamp and J. Mannhart, Rev. Mod. Phys. **74**, 485 (2002).
[31] C. Renner *et al.*, Nature (London) **416**, 518 (2002).
[32] A. Ohtomo *et al.*, Nature (London) **419**, 378 (2002).
[33] B. W. Smith, D. E. Luzzi, and Y. Achiba, Chem. Phys. Lett. **331**, 137 (2000).
[34] K. Suenaga *et al.*, Phys. Rev. Lett. **90**, 055506 (2003).